Journal of Electrical and Computer Engineering Innovations
(JECEI)
Journal homepage: http://www.jecei.sru.ac.ir

Research paper

Utilization of CHB Multilevel Inverter for Harmonic Reduction in Fuzzy Logic Controlled Multiphase LIM Drives

P. Hamedani [1,2*]***, A. Shoulaei*** [1]

[1]*Department of Electrical Engineering, Iran University of Science & Technology, Tehran, Iran.*

[2]*Department of Railway Engineering and Transportation Planning, University of Isfahan, Isfahan, Iran.*

Article Info

Article History:

Received 30 March 2019
Reviewed 08 June 2019
Revised 30 August 2019
Accepted 08 December 2019

Keywords:

CHB inverter
Fuzzy Logic Controller
Linear Induction Motor (LIM)
Multiphase LIM
Total Harmonic Distortion
Interharmonics

[*]Corresponding Author's Email Address:
p.hamedani@eng.ui.ac.ir

Abstract

Background and Objectives: Despite superior privileges that multiphase motors offer in comparison with their three-phase counterparts, in the field of multiphase linear induction motors (LIMs) few studies have been reported until now. To combine the advantages of both multiphase motors and linear induction motors, this paper concentrates on multiphase LIM drives considering the end effects.

Methods: The main contributions of this paper can be divided into two major categories. First, a comparative study has been conducted about the dynamic performance of Fuzzy Logic Controller (FLC) and Genetic-PI controller for a seven-phase LIM drive; and second, because of the superior performance of the FLC method revealed from the results, the harmonic pollution of the FLC based LIM drive has been studied in the case of supplying through a five-level Cascaded H-bridge (CHB) VSI and then compared with the traditional two-level VSI fed one.

Results: The five-level CHB-VSI has utilized a multiband hysteresis modulation scheme and the two-level VSI has used the traditional three-level hysteresis modulation strategy. Note that for harmonic distortion assessment both harmonic and interharmonic components are considered in THD calculations.

Conclusion: The results validate the effectiveness of the proposed FLC for seven-phase LIM drive supplied with five-level CHB-VSI and guarantee for perfect control characteristics, lower maximum starting current, and significant harmonic and interharmonic reduction.

Introduction

From the beginning of this century, multiphase motor drives have attracted worldwide attention due to the significant advantages they have in comparison with three-phase motors [1]. The predominant benefits of using multiphase machines are greater torque density, increase in efficiency, lower torque pulsation, higher fault tolerance, and lower required rating per inverter leg (which results in simpler and more reliable power electronics devices) [2]. Furthermore, multiphase motors possess additional degrees of freedom by which more than one motor can be independently controlled through a single Voltage Source Inverter (VSI) [2]-[4]. For this purpose, the stator windings of the motors must have an appropriate connection style [2]-[4]. The dominant advantage of this concept is that the number of inverter legs decreases.

Although this idea is appropriate for all types of multiphase AC machines, until now, the most research interests in the area of multiphase machines are concentrated on AC rotational machines [1]-[12]. Consequently, in this paper, an attempt is made to provide a survey in control of multiphase LIMs with more than three phases.

Additionally, Linear Induction Motors (LIMs) are extensively utilized in industrial applications and high-speed transportation systems because of the significant privileges they offer. Nevertheless, accurate modeling of these machines is more complicated than the rotational induction ones due to the end effects [13]-[16].

A famous per-phase model of the LIM was proposed by Duncan [17]. This model was extracted by appropriate modification of the traditional rotary induction machine model. To reflect the end effects, the magnetizing branch was suitably modified [17]. Despite the usefulness and simplicity of this model, it was not directly applicable to drive applications. In [18] using Duncan's equivalent circuit model and regarding the end effect phenomena, the dynamic model of the three-phase LIM was suggested. Nevertheless, the end effect has been just regarded in the direct-axis equivalent circuit. The quadrature-axis equivalent circuit of the motor has been considered the same as a RIM with no end effect. However, it is explicit that for precise modeling of a LIM, both direct and quadrature axes must be affected by the end effect. Six years later, the second author of [18] introduced another dynamic model for three-phase LIM including the end effect in both direct and quadrature axes of the model [19]. In [20], regarding the end effect phenomena, the dynamic model of multiphase LIM has been derived for more than three phases. This model has been extracted by choosing an arbitrary rotating reference-frame and utilizing Park's transformation. On the other hand, among various control techniques accomplished on the LIM, Indirect Field Oriented Control (IFOC) method is an approved control strategy abundantly utilized for LIM drive applications [19]-[23]. The principal concept behind IFOC of a LIM is based on the alliance of the secondary flux vector with the direct-axis, which leads to the decoupling of flux and thrust [19]-[23]. To achieve this, the component of secondary flux along the quadrature-axis must be set to zero. Furthermore, the component of secondary flux along the direct-axis must be fixed on the nominal secondary flux value.

Moreover, in the past decade, multi-level inverters (MLIs) have been extensively utilized due to their particular privileges in power quality improvement [24]-[25]. The principal preferences of MLIs are lower voltage stress (dv/dt) on power electronic switches and reduced voltage harmonics of the VSI.

Therefore, it would be an interesting idea to use multilevel inverters for supplying LIM drives. An investigation of various topologies and control methods for multilevel inverters is presented in [24]-[25]. Cascaded H-bridge (CHB) inverter is a well-known multilevel structure utilized in high-power Medium-Voltage (MV) drives. The CHB inverter, in comparison with other multilevel inverters, has a simpler and modular topology. In recent years, CHB-VSIs have been extensively utilized in electrical motor drive applications due to their prominent benefits in the reduction of harmonic contents and power quality enhancement [26]-[29]. A multiband hysteresis switching scheme for current control of CHB-VSIs has been suggested in [30]. Implementation of current control using the hysteresis method is simple and has a fast dynamic response [30]. Also, it shows suitable robustness performance. Moreover, to calculate the hysteresis bandwidth with respect to the CHB switching frequency, a frequency-domain strategy has been proposed [30]. As a result, the CHB multilevel inverter has been selected in this paper for supplying the multiphase LIM drive. According to above mentioned, the principal scope of this paper is to investigate the harmonic reduction of Fuzzy Logic Controlled (FLC) multiphase LIM drive fed through a five-level CHB-VSI in comparison with the traditional two-level VSI. The remainder of this paper is organized as follows. In the next section, the dynamic model for the n-phase LIM is presented considering the end effect phenomena in the magnetizing branch inductance. Then, the indirect field-oriented control of n-phase LIM regarding the end effect is demonstrated. Next, the CHB-VSI with multiband hysteresis switching scheme is illustrated. After that, the calculation of the Total Harmonic Distortion (THD) factor considering harmonic and interharmonic components will be discussed. The overall control system, the Genetic-PI based controller, and the fuzzy logic controller will be introduced in the next sections, respectively. Subsequently, the simulation results are provided for a seven-phase LIM drive. Finally, the conclusions are given.

Dynamic Modeling of The LIM Considering The End Effect

The per-phase model of a LIM developed by Duncan is depicted in Fig. 1.

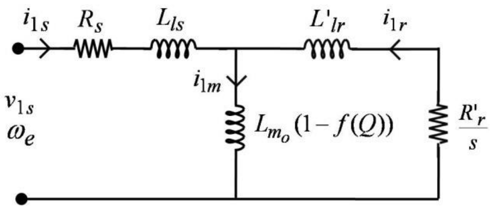

Fig. 1: The per-phase equivalent circuit model of LIM.

To take into account the end effect, a dimensionless factor Q and a function $f(Q)$ are defined as follows [17], [31]:

$$Q \cong \frac{D.R'_r}{L'_r.v_r} \quad (1)$$

$$f(Q) = \frac{\left(1-e^{-Q}\right)}{Q} \quad (2)$$

where D and v_r are the LIM length and speed, respectively. L'_r and R'_r are the self-inductance and resistance of the secondary, respectively.

Accordingly, the magnetizing branch is changed to $L_{m_0}\left(1-f(Q)\right)$, in which L_{m_0} is the magnetizing inductance when the LIM speed is equal to zero [17].

By applying the Park's transformation to Duncan's model, the dynamic model of an n-phase LIM can be extracted as follows [20]:

Primary voltage equations:

$$\begin{aligned}
v_{qs} &= R_s i_{qs} + \omega\lambda_{ds} + p\lambda_{qs} \\
v_{ds} &= R_s i_{ds} - \omega\lambda_{qs} + p\lambda_{ds} \\
v_{x1s} &= R_s i_{x1s} + p\lambda_{x1s} \\
v_{y1s} &= R_s i_{y1s} + p\lambda_{y1s} \\
&\vdots \\
v_{0s} &= R_s i_{0s} + p\lambda_{0s}
\end{aligned} \quad (3)$$

Secondary voltage equations:

$$\begin{aligned}
v_{qr} &= R'_r i_{qr} + (\omega-\omega_r)\lambda_{dr} + p\lambda_{qr} = 0 \\
v_{dr} &= R'_r i_{dr} - (\omega-\omega_r)\lambda_{qr} + p\lambda_{dr} = 0 \\
v_{x1r} &= R'_r i_{x1r} + p\lambda_{x1r} = 0 \\
v_{y1r} &= R'_r i_{y1r} + p\lambda_{y1r} = 0 \\
&\vdots \\
v_{0r} &= R'_r i_{0r} + p\lambda_{0r} = 0
\end{aligned} \quad (4)$$

Primary flux linkage equations:

$$\begin{aligned}
\lambda_{qs} &= L_{ls} i_{qs} + L_m\{1-f(Q)\}(i_{qs}+i_{qr}) \\
\lambda_{ds} &= L_{ls} i_{ds} + L_m\{1-f(Q)\}(i_{ds}+i_{dr}) \\
\lambda_{x1s} &= L_{ls} i_{x1s} \\
\lambda_{y1s} &= L_{ls} i_{y1s} \\
&\vdots \\
\lambda_{0s} &= L_{ls} i_{0s}
\end{aligned} \quad (5)$$

Secondary flux linkage equations:

$$\begin{aligned}
\lambda_{qr} &= L'_{lr} i_{qr} + L_m\{1-f(Q)\}(i_{qs}+i_{qr}) \\
\lambda_{dr} &= L'_{lr} i_{dr} + L_m\{1-f(Q)\}(i_{ds}+i_{dr}) \\
\lambda_{x1r} &= L'_{lr} i_{x1r} \\
\lambda_{y1r} &= L'_{lr} i_{y1r} \\
&\vdots \\
\lambda_{0r} &= L'_{lr} i_{0r}
\end{aligned} \quad (6)$$

where $p \equiv d/dt$ and ω_r denotes the secondary angular speed. Also, ω-ω_r represents the slip angular frequency ($\omega-\omega_r \equiv \omega_{sl}$).

The LIM thrust can be expressed as [20]:

$$F = \frac{n}{2}\frac{\pi}{\tau}\left(\lambda_{qr} i_{dr} - \lambda_{dr} i_{qr}\right) \quad (7)$$

in which τ represents the motor pole pitch.

Indirect Field-Oriented Control of LIM Considering End Effects

The main idea behind the IFOC of a LIM is based on aligning the reference frame to the secondary flux vector, which results in the decoupling of flux and thrust. Consequently, the component of secondary flux along the quadrature-axis must be set to zero. In other words, the secondary flux vector should be aligned with the direct-axis and its value must be fixed on the nominal secondary flux value. It follows that [20]:

$$\lambda_{qr} = 0 \quad \text{and} \quad \frac{d\lambda_{qr}}{dt} = 0 \quad (8)$$

Supposing $v_{qr} = v_{dr} = 0$, the slip angular frequency ($\omega_{sl} \equiv \omega_e - \omega_r$) will be calculated using (4) and (6) and by omitting the i_{qr} as:

$$\omega_{sl} = R'_r \left[\frac{1-f(Q)}{\frac{L'_{lr}}{L_m} + (1-f(Q))}\right] \times \frac{i_{qs}}{\lambda_{dr}} \quad (9)$$

Using (4) and (6) and by omitting i_{dr}, the direct-axis secondary flux (λ_{dr}) will be calculated:

$$\lambda_{dr} = \frac{L_m(1-f(Q))}{1+\left\{\frac{L'_{lr}+L_m(1-f(Q))}{R'_r}\right\}p} \times i_{ds} \quad (10)$$

It is notable that supposing $v_r \approx 0$ and $f(Q) \approx 0$, will result in $\omega_{sl} \approx R'_r L_m i_{qs}/(L'_r \lambda_{dr})$ and $\lambda_{dr} \approx L_m i_{ds}/\left(1+\left(L'_r/R'_r\right)p\right)$ (where $L'_r = L'_{lr} + L_m$), which are in accordance with rotary induction motors. The LIM thrust could be written as [20]:

$$F = \frac{n}{2}\frac{\pi}{\tau}\frac{L_m\left(1-f(Q)\right)}{L'_{lr}+L_m\left(1-f(Q)\right)}\lambda_{dr} i_{qs} \quad (11)$$

Cascaded H-Bridge Multilevel Inverter With Multiband Hysteresis Switching Scheme

In Fig. 2, the basic structure of a single-phase five-level CHB-VSI is illustrated with two cascaded H-Bridge (HB) cells. Each of the semiconductor switching devices S_{11}, S_{12}, …, S_{22} represents an IGBT with back-to-back diode. The CHB-VSI output voltage can be written as $V_c = u(t) \times V_{dc}$, in which $u(t)$ is the output logic signal including five different levels. In Fig. 3 the flowchart of five-band hysteresis switching scheme is represented. In this figure, the current error is defines as $C_e=i_s-i_s^*$, in which i_s and i_s^* represent the actual and reference phase currents, respectively. Also, h denotes the hysteresis band. The modulation scheme produces five voltage levels, i.e. u = -1, -1/2, 0, +1/2, +1.

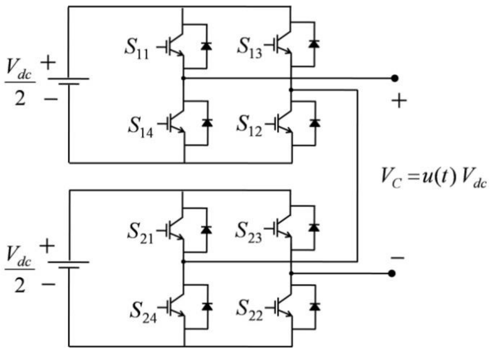

Fig. 2: Five-level CHB-VSI.

For an n-phase voltage source inverter with n-phase balanced load, the instantaneous values of phase-to-neutral voltages (V_1 , ..., V_n) can be written as a function of DC bus voltage V_{dc} and logic variables (u_1, ..., u_n) as:

$$\begin{bmatrix} v_1 \\ v_2 \\ \vdots \\ v_{n-1} \\ v_n \end{bmatrix} = \frac{V_{dc}}{n} \begin{bmatrix} n-1 & -1 & -1 & \cdots & -1 \\ -1 & n-1 & -1 & \cdots & -1 \\ -1 & -1 & \ddots & \cdots & -1 \\ \vdots & \vdots & \cdots & \vdots & \vdots \\ -1 & -1 & \cdots & n-1 & -1 \\ -1 & -1 & \cdots & -1 & n-1 \end{bmatrix}_{n\times n} \begin{bmatrix} u_1 \\ u_2 \\ u_3 \\ \vdots \\ u_{n-1} \\ u_n \end{bmatrix} \tag{12}$$

For a five-level CHB-VSI, each logic variable (u_1,... , u_n) has five levels of output, i.e. u_i = -1, -1/2, 0, +1/2, +1, according to the five-band hysteresis switching flowchart.

Harmonic and Interharmonic Distortion

Generally, power quality evaluations are performed on periodic voltages and current waveforms. The defined criteria are usually expressed with regard to the harmonic and fundamental components of the waveforms. Unfortunately, currents waveforms in many industrial loads are not periodic. For instance, the current waveform generated by the hysteresis modulation possesses (except the fundamental sinusoidal component), random and stochastic components that are irregular and non-periodic. Consequently, the custom power quality criteria which are defined based on the periodicity of the signals, could not be utilized. Nevertheless, in the past decade, considerable research has been concentrated on solving this issue [32]. Analyzing non-periodic loads is mostly based on the time windows utilized for extracting statistical data to achieve an overall characteristic. The IEC 61000-4-30 recommends a window width of about 200ms, which corresponds to 10 cycles on 50 Hz systems and 12 cycles on 60 Hz systems [32].

According to the IEC 61000-4-30, considering a 200ms time window is appropriate [32]. This window width is 10 cycles on 50 Hz systems and 12 cycles on 60 Hz systems. The stochastic nature of controller operation dictates that the hysteresis modulation will result in harmonic, interharmonic, and subharmonic distortion. Unlike harmonics which are located on multiples of the fundamental frequency, interharmonics and subharmonics take place at non-integer multiples of the fundamental frequency.

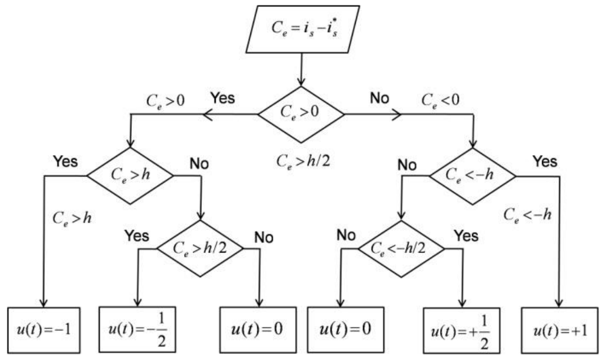

Fig. 3: Flowchart of the five-band hysteresis modulation.

Interharmonics and subharmonics take place at non-integer multiples above or below the fundamental frequency, respectively. To avoid complexity, in the remainder of this work, interharmonics and subharmonics are classified into a single group, called interharmonic distortion.

It is notable that for calculating the Total Harmonic Distortion (*THD*), when interharmonics exist, two components should be considered [32]:

$$THD = \sqrt{TDHD^2 + TIHD^2} \tag{13}$$

TDHD and *TIHD* denote the total discrete harmonic distortion and the total interharmonic distortion, respectively. For a current signal, *TDHD* and *TIHD* are written as [32]:

$$TDHD_I = \frac{\sqrt{\sum_{m=2}^{m_{\max}} I_m^2}}{I_1} \tag{14}$$

$$TIHD_I = \frac{\sqrt{\sum_{m=0}^{m_{\max}-1} IRSS_{m,m+1}^2}}{I_1} \tag{15}$$

where m is the harmonic order and m_{max} represents the maximum harmonic order. I_1 is the fundamental value of current waveforms. *IRSS* is the root sum squared value of the current interharmonics which are located between two consecutive harmonics m and m+1 [32]. If the LIM drive operates at a frequency of f_1, by considering a frequency resolution of Δf, the *IRSS* can be determined as [32]:

$$IRSS_{m,m+1} = \sqrt{\sum_{f=f_1 \cdot m+\Delta f}^{f_1 \cdot (m+1)-\Delta f} IRSS_{m,m+1}^2} \tag{16}$$

Consequently, for a current waveform including harmonics and interharmonics, the equivalent *THD* index ($THD_{e\text{-}I}$) is defined as [32]:

$$THD_{e-I} = \frac{\sqrt{\sum_{m \neq 1}^{m_{max}} I_m^2 + \sum_{m=0}^{m_{max}-1} \sum_{f=f_1 \cdot m+\Delta f}^{f_1 \cdot (m+1)-\Delta f} I_m^2}}{I_1} \tag{17}$$

where I_m denotes the rms values of the current harmonics and interharmonics. For voltage waveforms, the equivalent *THD* index ($THD_{e\text{-}V}$) can be calculated in the same way.

Control System

The total IFOC diagram of the n-phase LIM drive is demonstrated in Fig. 4. The LIM is fed through CHB-VSI based multiband hysteresis switching strategy. The end effect is regarded in the LIM model and the controller. A current control loop and a speed control loop are included in the LIM drive. In this work, both genetic-PI based controller and fuzzy Logic Controller are utilized as regulators in the speed control loop.

In this work, both genetic-PI based controller and fuzzy Logic Controller are utilized as regulators in the speed control loop.

The command quadrature-axis primary current (i_{qs}^*) is produced by the speed controller. Also, the command direct-axis primary current (i_{ds}^*) is produced according to the nominal direct-axis secondary flux (λ_{dr}^*) and the LIM speed. Moreover, the gains K_1 and K_2 are calculated from (9) and (10). Note that K_1 and K_2 are dependent on $f(Q)$ and thus dependant on the LIM speed [33]. The command currents (i_{1s}^*, i_{2s}^*, …, i_{ns}^*) are produced using i_{qs}^* and i_{ds}^* and by applying inverse Park's transformation. The current controller produces the firing pulses for the CHB-VSI switches. For reducing the harmonic and interharmonic distortion of the multiphase LIM drive, a five-level CHB-VSI (with two HB cells) has been unutilized and compared with the conventional two-level VSI.

The current controller produces the firing pulses for the CHB-VSI switches. For reducing the harmonic and interharmonic distortion of the multiphase LIM drive, a five-level CHB-VSI (with two HB cells) has been unutilized and compared with the conventional two-level VSI.

Genetic-PI Based Controller [34]

Genetic Algorithm (GA) is a well-known optimization method, inspired by the populations evolve in nature. In this paper, GA has been utilized for optimizing the PI gains of the speed controller.

For GA implementation, the roulette-wheel selection function has been used. Moreover, the two-point crossover with a probability of 0.80 is chosen.

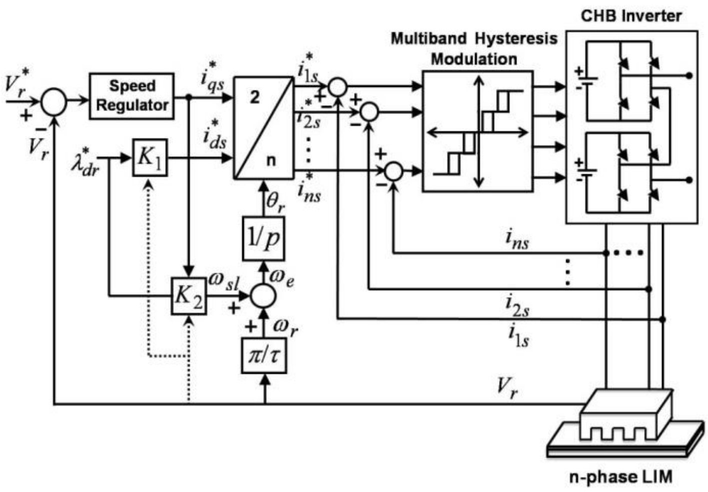

Fig. 4: Block diagram of the proposed IFOC scheme for n-phase LIM.

To avoid local minimum answers, the adaptive feasible mutation has been selected. Furthermore, the population size is considered 200 chromosomes for each generation.

The objective function, which must be minimized, is the sum of different functions. In this paper, rise time, settling time, maximum overshoot, steady-state error, and load change error are taken into account in the objective function, as follows [34]:

$$F_{obj} = k_1.F_{obj_1} + k_2.F_{obj_2} + k_3.F_{obj_3} + k_4.F_{obj_4} + k_5.F_{obj_5} \tag{18}$$

where $F_{obj_1} = \frac{T_r}{M_T} + P$

$$F_{obj_2} = \frac{T_S}{M_T} + P \qquad F_{obj_3} = \frac{M_p}{M_E} + P$$

$$F_{obj_4}=\frac{|E_{SS}|}{M_E}+P \qquad F_{obj_5}=\frac{|F_L|}{M_L}+L \tag{19}$$

k_1 to k_5 are the importance coefficients and are chosen as: $k_1=k_2=k_3=k_4=k_5=1$. E_{SS}, M_p, T_r, and T_S denote the steady-state error, the overshoot, the rise time, and the settling time, respectively. The constants M_T, M_E, and M_L are scaling factors. In this research, these constants are considered as M_T = t_{final}, M_E = y_d, M_L = 1 (t_{final} and y_d denote the total time and the desired LIM speed, respectively). P and L are penalty factors that must be set to zero in case of a stable speed response. Moreover, to minimize the effect of load variations on the speed response, the load change error is also considered to the objective function as $F_L=y_{(t_{final})}(full-load)-y_{(t_{final})}(no-load)$. For small load change errors, penalty factor L is set to zero and for high error values, it is considered 8. If the LIM speed becomes unstable or deficient, the parameters are selected according to Table 1 [34].

Finally, as the main goal of this paper is controlling the LIM drive in the whole speed range, the final objective function optimized by GA is considered as:

$$F_{obj_{Total}}=F_{obj}(V_r=V_{rated})+F_{obj}(V_r=\frac{V_{max}}{2}) \tag{20}$$

In the Appendix, the optimized PI controller gains obtained from GA are given. Moreover, the best objective functions in each generation, during the GA optimization process, are captured and demonstrated in the Appendix.

Table 1: Parameters of the objective function in deficient and unstable conditions [34]

	E_{SS}	T_S	T_r	M_P	P
Deficient condition	$y_d-y_{(t_{final})}$	M_T	M_T	0	7
Unstable condition	y_d	M_T	T_r	y_d	10

Fuzzy Logic Controller (FLC)

In Fig. 5, the total IFOC diagram of the multiphase LIM drive with FLC is demonstrated. The linguistic variables of FLC are selected according to the LIM model [23]. The speed error $\Delta V_r(n)$ and the change of speed error $\Delta e(n)$ are considered as the inputs of the FLC. The output variable is the command LIM force ($F_e^*(n)$).

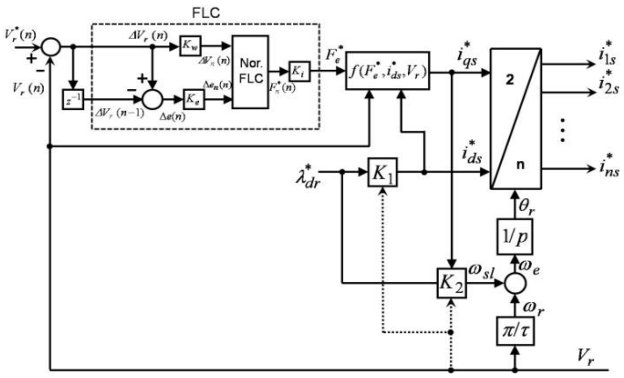

Fig. 5: Block diagram of the proposed FLC for IFOC of n-phase LIM.

Correspondingly, the command quadrature-axis current (i_{qs}^*) will be produced using (11). In the next step, the scaling factors K_ω, K_e, and K_i are chosen by trial-and-error to get optimal drive performance.

For FLC implementation, the Mamdani-type fuzzy inference approach and the center of gravity defuzzification method are used [23].

The FLC rules, used in this work, are as follows [23]:

If ΔV_n is PH (Positive High), then F_e^* is PH.

If ΔV_n is ZE (Zero) and Δe is PO (Positive), then F_e^* is PL.

If ΔV_n is ZE and Δe is NE (Negative), then F_e^* is NC (No Change).

If ΔV_n is ZE and Δe is ZE, then F_e^* is NC.

If ΔV_n is NL (Negative Low), then F_e^* is NL.

If ΔV_n is NH (Negative High), then F_e^* is NH.

The membership functions of FLC are illustrated in Fig. 6.

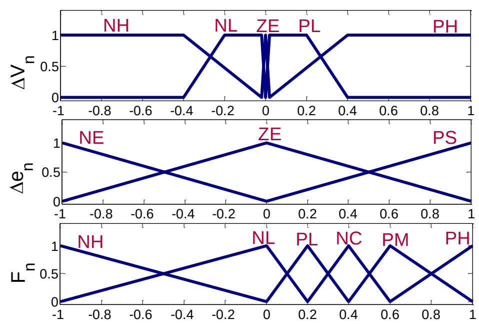

Fig. 6: Fuzzy logic membership functions; speed error ΔV_n, speed error change Δe_n, command LIM thrust $F_{en}^*(n)$.

Results and Discussion

To investigate the functionality of the proposed FLC of LIM drive with the end effect considerations, different tests have been performed at various operating points. The validity of the suggested LIM model combined with the relevant controller is evaluated by simulating a seven-phase LIM drive. The seven-phase LIM is fed through a five-level CHB-VSI with a five-band hysteresis switching technique. The performance validation of the FL controller and Genetic-PI Based controller have been evaluated and compared with each other. The speed and current responses have been monitored under various operating situations such as abrupt changes in reference speed, step changes in load, and also at various reference speeds and loads. The simulation of the complete drive has been executed utilizing Matlab/Simulink software with the parameters expressed in the Appendix. Furthermore, the power quality improvement of the seven-phase LIM drive supplied with five-level CHB-VSI is studied and compared with the traditional two-level VSI. For this purpose, the THD index has been evaluated for both inverter topologies considering both harmonics and interharmonics. Some of the achieved results are presented in the following paragraphs.

In the CHB-VSI, a net dc-link voltage of $V_{dc}=90V$ is considered for each HB cell. Also, a hysteresis band of $h\approx 0.1A$ is applied.

The FL controller gains are chosen to achieve the best transients and dynamic responses considering the requirement of stability. The command speed and dynamic speed response of the LIM drive for Genetic-PI and FL controllers are demonstrated in Figs. 7 (a)-(b), respectively. First, the LIM is driven at 0.5 m/sec command speed and with no external force. At t=3 sec, the command speed is suddenly increased from 0.5 to 1.5 m/sec. At t=6 sec, a 100 N external force is applied to the LIM. At t=9 sec, the command speed is suddenly decreased from 1.5 to 1 m/sec while keeping constant the external force at 100 N. The external force applied to the motor primary is decreased at t=12 sec from 100 N to 50 N. Despite optimum adjusting of PI constants utilizing GA, the FLC showed better performance from the viewpoint of dynamic response time, overshoot, and adaptability to external force changes.

Figs. 8 (a)-(b) illustrate the corresponding LIM primary phase currents for PI and FL controllers, respectively. From these figures, the maximum starting current for PI and fuzzy are equal to 6.64 A and 3.96 A, respectively. As a result, it is clear that FLC has lower starting current in comparison with PI controller, which increases the motor ability and decrease the inverter rating.

Furthermore, a quantitative comparison of some dynamic response parameters for the aforementioned control methods is illustrated in Table 2 for a command speed of 1.5 m/sec.

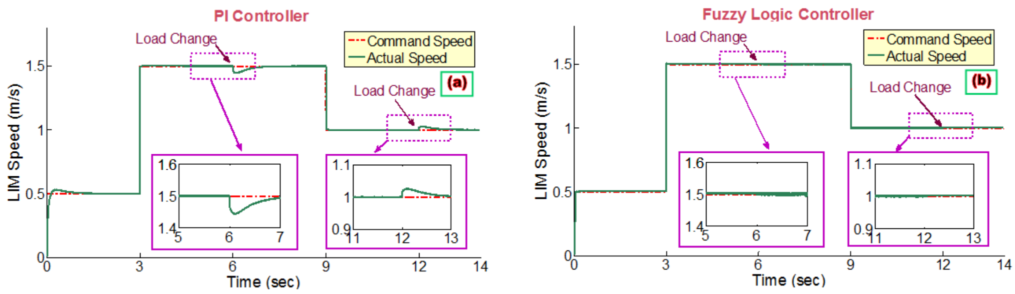

Fig. 7: Command speed and actual speed of the LIM drive; (a) Genetic-PI controller and (b) Fuzzy logic controller.

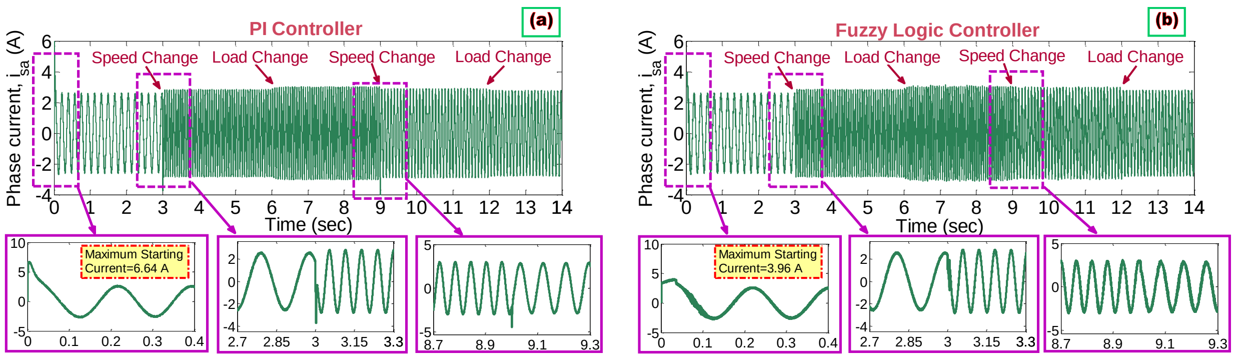

Fig. 8: Primary current of the LIM drive; (a) Genetic-PI controller and (b) Fuzzy Logic controller.

According to the results, it is obvious that in the FLC of multilevel LIM drive, the actual LIM speed tracks the command speed under various loading conditions. Moreover, it offers more accurate dynamic responses, which makes it suitable for high performance drive applications.

Table 2: Dynamic response parameters of Genetic-PI and Fuzzy Logic Controller

		I_{strat} [A]	E_{ss} [%]	M_P [%]	T_r [sec]
No-Load	Genetic-PI	0.11	3%	0.06	8.98
	Fuzzy	0.06	0	0.06	4.47
F_L=100N	Genetic-PI	0.25	0.2	0.03	8.98
	Fuzzy	0.09	0	0.03	4.53
F_L=150N	Genetic-PI	1.5	0	≈ 0	8.98
	Fuzzy	0.11	0	≈ 0	4.57

In the next step, the THD index of the seven-phase LIM drive supplied with five-level CHB-VSI with five-band hysteresis modulation is studied and compared with the traditional two-level VSI. THD index has been evaluated for both topologies considering both harmonic and interharmonic components.

Unlike power system analysis in which the power frequency is almost considered constant (i.e. 50 Hz), in variable speed drives the inverter frequency is variant and dependent on the reference speed and external loading condition. Thus, at first, the fundamental frequency should be computed. Then, according to the fundamental frequency, the harmonic and interharmonic components should be extracted from the frequency spectrum of the signal. Consequently, the THD index can be calculated from (17). For harmonic analysis and evaluation of the fundamental component (frequency and amplitude), a time window equal to 10 seconds (in steady-state operating condition) has been considered to achieve 0.1 Hz frequency resolution. The time step of the simulation (the data sampling time) has been considered equal to 50 microseconds. For THD calculations, THD parameters were calculated using time windows with the length of 10 cycles of the fundamental frequency (f_1) according to the IEC 61000-4-30 standard [35]. Thus, the frequency resolution will be equal to 1/TW (where TW=10/f_1 is time window length). In this paper, harmonics and interharmonics were calculated utilizing Fast Fourier Transform (FFT) on the time domain waveforms obtained from the simulation. Total simulation time of 14 seconds has been considered to have more accurate THD values with higher precision. Afterward, the results of the first 3 seconds (from 14 seconds) were omitted to guaranty the steady-state operation of the drive. Then, the remaining 11 seconds have been divided into time windows (9 or 10 time windows depending on f_1). Each window length was considered equal to 10 times of f_1 according to the IEC 61000-4-30 [35]. Consequently, for each waveform different THD values related to the different time windows have been extracted and the minimum, maximum, and mean of THD values have been recorded.

In Fig. 9 (a), the seven-phase LIM phase current and phase voltage supplied with five-level CHB-VSI (for h=0.5 A) at 1.5 m/s command speed and 100 N external force are shown. Similarly, the seven-phase LIM phase current and phase voltage supplied with the traditional two-level VSI for the same operating conditions is presented in Fig. 9 (b). It is obvious that in LIM drive fed through the CHB-VSI, waveforms are more sinusoidal in comparison with the ones fed through the two-level VSI. In Addition, for h=0.5 A, the average switching frequency (f_s) of the CHB and traditional VSI semiconductor switching devices are computed and illustrated in these figures which are equal to 206 Hz and 86 Hz, respectively. By decreasing the hysteresis band, the average switching frequency will increase. For h=0.1 A, the average switching frequency of the CHB and traditional VSI switching devices are 1594 Hz and 290 Hz, respectively

Figs. 10 (a)-(b) display the frequency spectrums of the LIM phase voltage for both CHB-VSI and traditional VSI. To show more clearly the frequency spectrum, the spectrums are depicted separately for both lower frequency components (top figure) and higher frequency components (bottom figure). Similarly, the frequency spectrums of the LIM phase current for both CHB and traditional VSI are illustrated in Figs. 11 (a)-(b). From these figures, the LIM phase voltage THD values for CHB and traditional VSI are equal to 28.01% and 45.90%, respectively. Correspondingly, the phase current THD values for CHB and traditional VSI are equal to 4.74% and 8.73%, respectively.

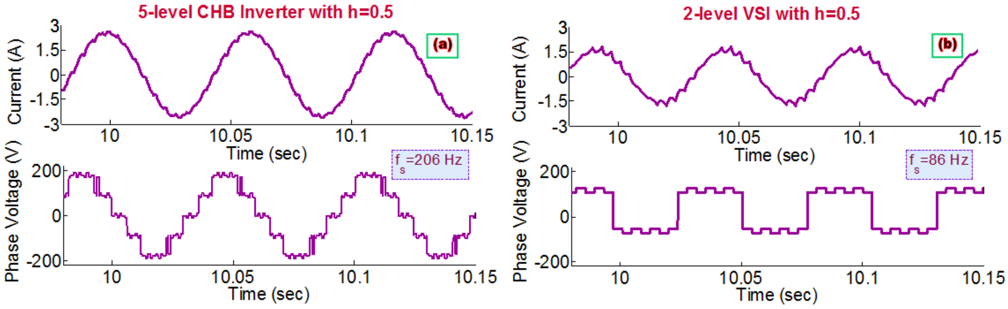

Fig. 9: The LIM phase current and phase voltage; (a) five-level CHB-VSI (b) two-level voltage source inverter.

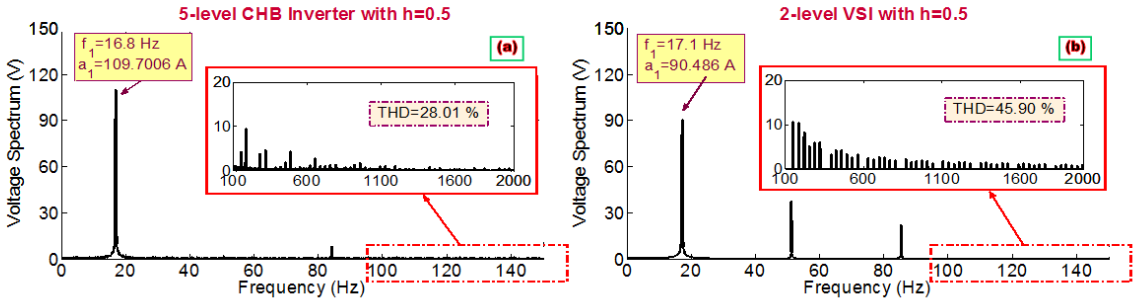

Fig. 10: The frequency spectrum of the seven-phase LIM phase voltage; (a) five-level CHB-VSI (b) two-level voltage source inverter.

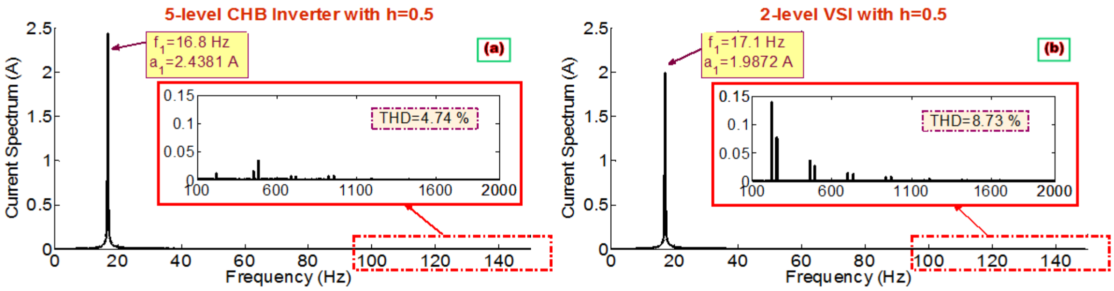

Fig. 11: The frequency spectrum of the seven-phase LIM current; (a) five-level CHB-VSI (b) two-level voltage source inverter.

It is clear from the figures that the magnitudes of harmonic and interharmonic components caused by the five-level CHB-VSI are significantly reduced in comparison with the two-level VSI. The THD indices of the LIM phase voltages and phase currents are computed for the CHB and the traditional VSI, different hysteresis bands, and different external forces. The seven-phase LIM drive was running with 0.9 m/sec command speed. Figs. 12-13 represent the THD indices of the LIM phase voltage and currents for The CHB and the traditional VSI, different hysteresis bands, and different external forces. Furthermore, the value of the calculated THD indices (in percent) and the fundamental component (amplitude and frequency) of the LIM phase voltages and currents are summarized in the Appendix.

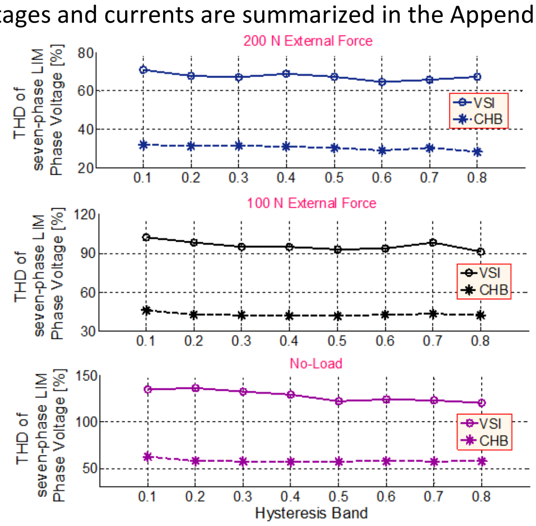

Fig. 12: Comparison of THD values [%] of the seven-phase LIM phase voltage supplied with five-level CHB and two-level VSI for different hysteresis bands and different external forces.

It is perceptible from the results that harmonic and interharmonic contents resulted from the five-level CHB-VSI are remarkably less than the traditional two-level VSI. Furthermore, generally by increasing the hysteresis band and by decreasing the external forces, the THD values will increase. It should be noted that if interharmonics are considered in THD calculations, the THD indices may have high values and even more than 100% in highly distorted conditions.

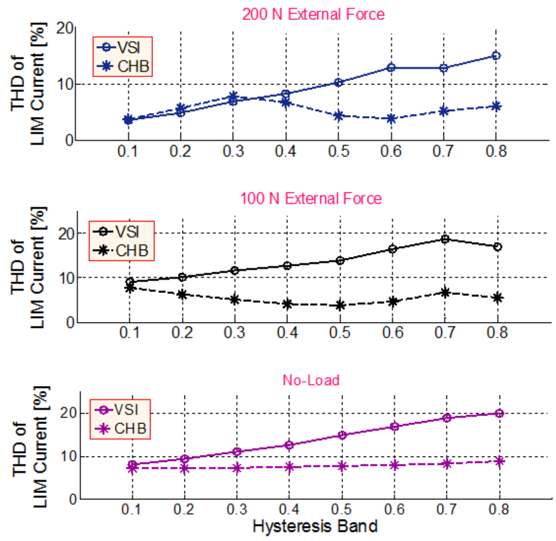

Fig. 13: Comparison of THD values [%] of the seven-phase LIM phase current supplied with five-level CHB and two-level VSI for different hysteresis bands and different external forces.

According to the results, it is evident that the FLC of seven-phase LIM drive offers perfect dynamic characteristics including fast and accurate speed response, which is also adaptive to the imposed external forces. Furthermore, the application of five-level CHB-VSI with five-band hysteresis modulation guarantees for lower THD indices and power quality improvement of the seven-phase LIM drive.

Conclusion

This paper presents a comparative study between the five-level Cascaded H-bridge (CHB) inverter and the traditional two-level VSI on the harmonic content of the multiphase linear induction motor drive with Fuzzy Logic Controller (FLC). Due to the existence of current a control loop in the multiphase LIM drive controlling diagram, the five-level CHB-VSI has utilized a multiband hysteresis modulation scheme and the two-level VSI has used the traditional three-level hysteresis modulation strategy. Since current waveforms generated by the hysteresis modulations possess random and stochastic components (except the fundamental sinusoidal component), the THD indices have been evaluated for both inverters considering both harmonic and interharmonic components. Simulation results manifest that the proposed Fuzzy Logic controller utilized for multiphase LIM drive presents satisfactory performance including fast response, no overshoot, negligible steady-state error, and lower maximum starting current. Furthermore, the applied five-level n-phase Cascaded H-bridge (CHB) VSI incorporating with multiband hysteresis modulation guarantees for harmonic and interharmonic reduction in the LIM drive.

Appendix

Fuzzy Logic controller gains: K_ω=0.008, K_e=0.05, K_i=1000
Genetic-PI controller gains: K_i=230.0118, K_p=84.3147

Table 3: LIM parameters

Phase voltage	240 V	R'_r	11.78 Ω
Current	5 A	L_{ls}	0.42 H
Power	1 HP	L'_{lr}	0.42 H
Pole pairs	2	L_m	0.4 H
Pole pitch	0.0465 m	λ^*_{dr}	0.9776 wb
Secondary length	0.82 m	M	4.775 kg
R_s	13.2 Ω	*Damping*	1 kg/s

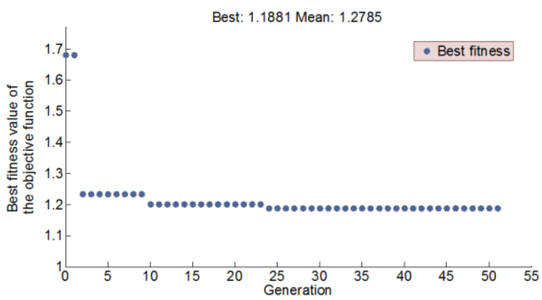

Fig. 14: The best objective functions in each generation during the optimization of PI gains using the genetic algorithm.

Author Contributions

This work is the continuations of the PhD thesis of P.Hamedani under supervision of Prof. A.Shoulaei. P.Hamedani carried out the data analysis, interpreted the results, and wrote the manuscript.

Acknowledgment

The authors gratefully thank the anonymous reviewers and the editor of JECEI for their useful comments and suggestions.

Conflict of Interest

The author declares that there is no conflict of interests regarding the publication of this manuscript. In addition, the ethical issues, including plagiarism, informed consent, misconduct, data fabrication and/or falsification, double publication and/or submission, and redundancy have been completely observed by the authors.

Abbreviations

D	LIM length
M	Primary weight
v_r	LIM speed
L'_r	Self-inductance of the secondary
R'_r	Resistance of the secondary
L'_{lr}	Leakage inductance of the secondary
R_s	Resistance of the primary
L_{ls}	Leakage inductance of the primary
L_{m0} (1-$f(Q)$)	Magnetizing inductance of LIM
ω_r	Secondary angular speed
ω	Synchronous angular speed
ω_{sl}	Slip angular frequency
F	LIM thrust
τ	Motor pole pitch
n	Number of phases
h	Hysteresis band
V_{dc}	DC bus voltage
u_1, …, u_{n}	logic variables
V_1 , …, V_{n}	Phase-to-neutral voltages
THD	Total Harmonic Distortion
TDHD	Total discrete harmonic distortion
TIHD	Total interharmonic distortion
m	Harmonic order
$m_{\max}$	Maximum harmonic order
IRSS	Root sum squared value of the current interharmonics
f_1	Fundamental frequency
Δf	Frequency resolution
i_{1s}^* , i_{2s}^* , …, i_{ns}^*	Command primary currents
i_{qs}^*	Command q-axis primary current
i_{ds}^*	Command d-axis primary current
λ_{dr}^*	Nominal d-axis secondary flux
k_1, …, k_5	Importance coefficients
E_{SS}	Steady-state error

M_p	Overshoot
T_r	Rise time
T_S	Settling time
M_T, M_E, M_L	Scaling factors
P and L	Penalty factors
$\Delta V_r(n)$	Speed error
$\Delta e(n)$	Change of speed error
F_{obj}	Objective function
F_e^*	Command LIM force
K_ω, K_e, K_i	Fuzzy Logic controller gains
K_i, K_p	Genetic-PI controller gains

References

[1] E. Levi, R. Bojoi, F. Profumo, H. A., Toliyat, S. Williamson, "Multi-phase induction motor drives- a technology status review," IET Electr. Power Appl., 1(4): 489-516, 2007.

[2] E. Levi, M. Jones, S. N. Vukosavic, H. A. Toliyat, "Operating principles of a novel multiphase multimotor vector-controlled drive," IEEE Transaction on Energy Conversion, 19(3): 508-517, 2004.

[3] E. Levi, M. Jones, S. N. Vukosavic, H. A. Toliyat, "A novel concept of a multiphase, multimotor vector controlled drive system supplied from a single voltage source inverter," IEEE Transaction on Power Electronics, 19 (2): 320-335, 2004.

[4] E. Levi, M. Jones, S. N. Vukosavic, "Even-phase multi-motor vector controlled drive with single inverter supply and series connection of stator windings," IEE Proc. Electric Power Applications, 150 (5): 580-590, 2003.

[5] M. Jones, S. N. Vukosavic, D. Dujic, E. Levi, "A synchronous current control scheme for multiphase induction motor drives," IEEE Transaction on Energy Conversion, 24(4): 860-868, 2009.

[6] H. Xu, H. A. Toliyat, L. J. Petersen, "Five-phase induction motor drives with DSP-based control system," IEEE Transaction on Power Electronics, 17 (4): 524-533, 2002.

[7] G. K. Singh, K. Nam, S. K. Lim, "A simple indirect field-oriented control scheme for multiphase induction machine," IEEE Transaction on Industrial Electronics, 52(4): 1177-1184, 2005.

[8] S. Williamson, S. Smith, "Pulsating torque and losses in multiphase induction machines," IEEE Transaction on Industry Applications, 39(4): 986-993, 2003.

[9] E. E. Ward, H. Harer, "Preliminary investigation of an inverter-fed 5-phase induction motor," Proceedings IEE, 116(6): 980-984, 1969.

[10] G. K. Singh, "Multi-phase induction machine drive research- a survey," International Journal of Electric Power system Research, 61: 139-147, 2002.

[11] E. Levi, A. Iqbal, S. N. Vukosavic, H. A. Toliyat, "Modeling and control of a five-phase series-connected two-motor drive," in Proc. of the IEEE Industry Electronics Society Annual Meeting-IECON, Roanoke, VA,:208-213, 2003.

[12] E. Levi, S. N. Vukosavic, M. Jones, "Vector control schemes for series-connected six-phase two-motor drive systems," IEE Proceedings Electric Power Applications, 152(2): 226-238, 2005.

[13] A. Shiri, A. Shoulaei, "Design Optimization and Analysis of Single-Sided Linear Induction Motor, Considering All Phenomena," IEEE Trans. on Energy Conversion, 27 (2): 516-525, 2012.

[14] M. R. Satvati, S. Vaez-Zadeh, "End-Effect Compensation in Linear Induction Motor Drives," Journal of power electronics, 11(5): 697-703, 2011.

[15] Y. Han, Z. Nie, J. Xu, J. Zhu, J. Sun, "Mathematical model and vector control of a six-phase linear induction motor with the dynamic end effect," Journal of power electronics, 20(2): 698–709, 2020.

[16] A. H. Selcuk, H. Kurum, "Investigation of End Effects in Linear Induction Motors by Using the Finite-Element Method," IEEE Transactions on Magnetics, 44(7): 1791-1795, 2008.

[17] J. Duncan, C. Eng, "Linear induction motor-equivalent-circuit model," IEE Proc. Power Application, 130(1): 51-57, 1983.

[18] K. Nam, J. H. Sung, "A new approach to vector control for linear induction motor considering end effects," in Proc. Of the IEEE Industry Applications Conference,: 2284-2289, 1999.

[19] G. Kang, K. Nam, "Field-oriented control scheme for linear induction motor with the end effect," IEE Proc. on Electric Power Appl., 152(1): 1565-1572, Nov. 2005.

[20] P. Hamedani, A. Shoulaie, J. M. M. Sadeghi, "Independent Control of Multiple Multiphase Linear Induction Motors Supplied From a Single Voltage Source Inverter," in Proc. of the 3rd International Conference on Recent Advances in Railway Engineering (ICRARE-2013), Tehran, Iran, May. 2013.

[21] J. Zhao, Z. Yang, J. Liu, T. Q. Zheng, "Indirect vector control scheme for linear induction motors using single neuron PI controllers with and without the end effects," in Proc. of the 7th Word Congress on Intelligent Control and Automation, china, : 5263-5267, 2018.

[22] E. F. Silva, E. B. Santos, P. C. M. Machado, M. A. A. Oliveira, "Vector control for linear induction motor," in Proc. of the 3rd IEEE International Conference on Industrial Technology (ICIT 2003), Maribor, Slovenia, :518-523, 2003.

[23] P. Hamedani, A. Shoulaie, "Modification of the field-weakening control strategy for linear induction motor drives considering the end effect," Advances in Electrical and Computer Engineering (AECE), 15(3): 3-12, 2015.

[24] J. Rodriguez, J. S. Lai, F. Z. Peng, "Multilevel Inverters: A Survey of Topologies, Controls, and Applications," IEEE Trans. Ind. Electron., 49, (4, :724-738, 2002.

[25] J. Rodriguez, S. Bernet, B. Wu, J. O. Pontt, S. Kouro, "Multilevel Voltage-Source-Converter Topologies for Industrial Medium-Voltage Drives," IEEE Trans. Ind. Electron., 54(6): 2930-2945, 2007.

[26] F. Khoucha, S. M. Lagoun, K. Marouani, A. Kheloui, M. E. H. Benbouzid, "Hybrid Cascaded H-Bridge Multilevel-Inverter Induction-Motor-Drive Direct Torque Control for Automotive Applications," IEEE Trans. Ind. Electron., 57(3), : 892-899, 2010.

[27] J. Rodriguez, L. Moran, P. Correa, C. Silva, "A Vector Control Technique for Medium-Voltage Multilevel Inverters," IEEE Trans. Ind. Electron., 49(4): 882-888, 2002.

[28] J. Wen, K. M. Smedley, "Hexagram Inverter for Medium-Voltage Six-Phase Variable-Speed Drives," IEEE Trans. Ind. Electron., 55(6), : 2473-2481, 2008.

[29] Z. Du, B. Ozpineci, L. M. Tolbert, J. N. Chiasson, J. N. "DC–AC Cascaded H-Bridge Multilevel Boost Inverter with No Inductors for Electric/Hybrid Electric Vehicle applications," IEEE Trans. Ind. Appl, 45(3): 963-970, 2009.

[30] R. Gupta, A. Ghosh, A. Joshi, "Multiband Hysteresis Modulation and Switching Characterization for Sliding-Mode-Controlled Cascaded Multilevel Inverter," IEEE Trans. Ind. Electron., 57(7): 2344-2353, 2010.

[31] A. Shiri, A. Shoulaie, "End effect braking force reduction in high-speed single-sided linear induction machine," International Journal of Energy Conversion and Management, Elsevier, 61: 43-50, 2012.

[32] A. Dehestani, S. Mohamadian, A. Shoulaie, "Unbalance Assessment and Apparent Power Decomposition in the Electric System of Interharmonic-producing Loads," European Transactions on Electrical Power. 24(2): 246-263, 2012.

[33] P. Hamedani, A. Shoulaie, "Indirect field oriented control of linear induction motors considering the end effects supplied from a cascaded H-bridge inverter with multiband hysteresis modulation," in Proc. of the 4th Power Electronics Drive Systems and Technologies Conference (PEDSTC), Tehran, Iran, :13-19, 2013.

[34] B. Mirzaeian, A. Kiyoumarsi, P. Hamedani, C. Lucas, "A new comparative study of various intelligent based controllers for speed control of IPMSM drives in the field-weakening region," International Journal of Expert Systems with Applications, Elsevier, 38(10): 12643-12653, 2011.

[35] M. H. J. Bollen, I. Y. H. Gu, "Signal Processing of Power Quality Disturbances," Piscataway, NJ, IEEE Press, :185-190, 2006.

Biographies

Pegah Hamedani was born in Isfahan, Iran, in 1985. She received B.Sc. and M.Sc. degrees from University of Isfahan, Iran, in 2007 and 2009, respectively, and the Ph.D. degree from Iran University of Science and Technology, Tehran, in 2016, all in Electrical Engineering. She is currently an Assistant Professor with the Department of Railway Engineering, University of Isfahan, Iran. Her research interests include power electronics, control of electrical motor drives, supply system of the electric railway (AC and DC), linear motors & MAGLEVs, and analysis of overhead contact systems. Dr. Hamedani was the recipient of the IEEE 11th Power Electronics, Drive Systems, and Technologies Conference (PEDSTC'20) best paper presentation award in 2020.

Abbas Shoulaei was born in Isfahan, Iran, in 1949. He received the B.Sc. degree from the Iran University of Science and Technology (I.U.S.T.), Tehran, Iran, in 1973, and the M.Sc. and Ph.D. degrees in electrical engineering from Universite des Sciences et Techniques du Languedoc (USTL), Montpellier, France, in 1981 and 1984, respectively. He is currently a Professor of Electrical Engineering with I.U.S.T. His research interests include power electronics, magnetic systems and linear motors, flexible ac current transmission systems, and high voltage dc.

How to cite this paper:

P. Hamedani, and A. Shoulaei, "Utilization of CHB Multilevel Inverter for Harmonic Reduction in Fuzzy Logic Controlled Multiphase LIM Drives," Journal of Electrical and Computer Engineering Innovations, 8(1): 19-30, 2020.

DOI: 10.22061/JECEI.2020.6664.355

URL: http://jecei.sru.ac.ir/article_1420.html